

# Molecular dynamics of linear molecules in strong magnetic fields

Cite as: J. Chem. Phys. **157**, 054106 (2022); <https://doi.org/10.1063/5.0097800>

Submitted: 02 May 2022 • Accepted: 12 July 2022 • Accepted Manuscript Online: 12 July 2022 •

Published Online: 04 August 2022

 Laurenz Monzel,  Ansgar Pausch,  Laurens D. M. Peters, et al.



View Online



Export Citation



CrossMark

## ARTICLES YOU MAY BE INTERESTED IN

[A new generation of effective core potentials from correlated and spin-orbit calculations: Selected heavy elements](#)

The Journal of Chemical Physics **157**, 054101 (2022); <https://doi.org/10.1063/5.0087300>

[Beyond GGA total energies for solids and surfaces](#)

The Journal of Chemical Physics **157**, 050401 (2022); <https://doi.org/10.1063/5.0107716>

[Zero-cost corrections to influence functional coefficients from bath response functions](#)

The Journal of Chemical Physics **157**, 054107 (2022); <https://doi.org/10.1063/5.0101396>

Lock-in Amplifiers  
up to 600 MHz



Zurich  
Instruments



# Molecular dynamics of linear molecules in strong magnetic fields

Cite as: J. Chem. Phys. 157, 054106 (2022); doi: 10.1063/5.0097800

Submitted: 2 May 2022 • Accepted: 12 July 2022 •

Published Online: 4 August 2022







View Online



Export Citation



CrossMark

Laurenz Monzel,<sup>1</sup>  Ansgar Pausch,<sup>1</sup>  Laurens D. M. Peters,<sup>2</sup>  Erik I. Tellgren,<sup>2</sup>  Trygve Helgaker,<sup>2</sup>   
and Wim Klopper<sup>1,a)</sup> 

## AFFILIATIONS

<sup>1</sup>Karlsruhe Institute of Technology (KIT), Institute of Physical Chemistry, KIT Campus South, P.O. Box 6980, D-76049 Karlsruhe, Germany

<sup>2</sup>Hylleraas Centre for Quantum Molecular Sciences, Department of Chemistry, University of Oslo, P.O. Box 1033 Blindern, N-0315 Oslo, Norway

<sup>a)</sup>Author to whom correspondence should be addressed: [klopper@kit.edu](mailto:klopper@kit.edu)

## ABSTRACT

Molecular rotations and vibrations have been extensively studied by chemists for decades, both experimentally using spectroscopic methods and theoretically with the help of quantum chemistry. However, the theoretical investigation of molecular rotations and vibrations in strong magnetic fields requires computationally more demanding tools. As such, proper calculations of rotational and vibrational spectra were not feasible up until very recently. In this work, we present rotational and vibrational spectra for two small linear molecules, H<sub>2</sub> and LiH, in strong magnetic fields. By treating the nuclei as classical particles, trajectories for rotations and vibrations are simulated from *ab initio* molecular dynamics. Born–Oppenheimer potential energy surfaces are calculated at the Hartree–Fock and MP2 levels of theory using London atomic orbitals to ensure gauge origin invariance. For the calculation of nuclear trajectories, a highly efficient Tajima propagator is introduced, incorporating the Berry curvature tensor accounting for the screening of nuclear charges.

© 2022 Author(s). All article content, except where otherwise noted, is licensed under a Creative Commons Attribution (CC BY) license (<http://creativecommons.org/licenses/by/4.0/>). <https://doi.org/10.1063/5.0097800>

## I. INTRODUCTION

The presence of a magnetic field affects the interactions among the nuclei and electrons that make up atoms and molecules. On Earth, these effects are small and can be accurately described using perturbation theory and response methods. Elsewhere in the universe, the effects of a magnetic field can be much stronger. In the atmosphere of a magnetic white dwarf star, for example, field strengths of the order of 100 000 T can be observed,<sup>1</sup> close to one atomic unit field strength,  $B_0 = \hbar/(ea_0^2) \approx 2.35 \times 10^5$  T. Under such conditions, magnetic interactions compete with the electric interactions, strongly affecting the electronic structure of atoms and molecules.<sup>2</sup>

The electronic structure of atoms in the presence of a magnetic field has been studied for decades, and theoretical predictions of spectral transitions have been used to map out the magnetic field strength on the surface of white dwarfs—see, for example, Ref. 3. The

theoretical description of molecules in a magnetic field is more complicated than that of atoms, and it is only during the past decade that a general study of molecules in a strong magnetic field has become possible. An essential step forward was the introduction of London atomic orbitals (LAOs) in a finite magnetic field, making it possible to study molecules in an arbitrary orientation relative to the magnetic field.<sup>4</sup> A number of such studies have now been published using special codes developed for such studies—calculations can now be carried out at all the standard levels of electronic structure theory, including Hartree–Fock theory,<sup>4–7</sup> full-configuration-interaction theory,<sup>8,9</sup> coupled-cluster theory,<sup>10–13</sup> density-functional theory,<sup>14–18</sup> and GW theory.<sup>19–21</sup> Non-Born–Oppenheimer calculations have also been carried out for atoms and molecules using explicitly correlated Gaussians.<sup>22–25</sup> Methods for analytical calculation of forces and geometry optimizations are available.<sup>6,18,26</sup> These studies have revealed a number of interesting features of molecules in a strong magnetic field, including the existence of a new bonding

mechanism, paramagnetic bonding, replacing covalent bonding as the chief mechanism for chemical bonding in an ultrastrong magnetic field.<sup>8</sup>

While much has been learned about molecular electronic structure and chemistry in a strong magnetic field, less is known about the dynamics of molecules in a magnetic field. Within the Born–Oppenheimer (BO) approximation, the theoretical foundation of *ab initio* molecular dynamics (MD) in a magnetic was laid more than 30 years ago by Schmelcher and co-workers<sup>27–29</sup> and by Mead and co-workers.<sup>30–32</sup> In particular, these authors discussed how the Lorentz force acting on the moving nuclei is screened by the electrons in the molecule, requiring the evaluation of the Berry curvature for all pairs of atoms in the system. The importance of the screening force was demonstrated by Ceresoli *et al.*,<sup>33</sup> who in 2007 calculated the Berry curvature of H<sub>2</sub> from a Hartree–Fock wave function in a minimal basis of Slater orbitals equipped with London phase factors. Using a parameterized BO potential, these authors presented the first molecular dynamics calculations with a screened London force for H<sub>2</sub> in a perpendicular field orientation.

The first general scheme for *ab initio* BO molecular dynamics was presented by Culpitt *et al.*<sup>34</sup> and Peters *et al.*<sup>35</sup> in 2021. Obtaining the Berry curvature by a finite-difference approach,<sup>34</sup> these authors calculated BO trajectories of He and H<sub>2</sub> at different field strengths at the Hartree–Fock level of theory in a basis of London Gaussian orbitals.<sup>35</sup> The trajectories were propagated using a series of new propagators and designed to include the nonconservative screened Lorentz forces in the dynamics in a stable and efficient manner. From the trajectories, rovibrational spectra of H<sub>2</sub> were calculated, revealing a number of features not observed in the field-free cases: couplings of rotations/vibrations with the cyclotron rotation, overtones with unusual selection rules, and hindered rotations that transmute into librations with increasing field strength. More recently, these authors have presented an analytical scheme for the evaluation of the screened Lorentz force.<sup>36</sup>

In this paper, we present more extensive studies of molecular dynamics in a strong magnetic field, introducing a highly efficient Tajima propagator for the trajectory calculations. Extensive molecular dynamics simulations of H<sub>2</sub> and LiH reveal a more detailed and complete picture of the rovibrational spectra of molecules in a magnetic field.

## II. THEORY

### A. Molecules in external magnetic fields

Within the framework of both Hamiltonian mechanics and quantum mechanics, the effect of an external magnetic field  $\mathbf{B}$  on a physical system such as a molecule can be considered through its magnetic vector potential  $\mathbf{A}$  as defined by  $\mathbf{B} = \nabla \times \mathbf{A}$ . Choosing the Coulomb gauge for the magnetic vector potential,  $\nabla \cdot \mathbf{A} = 0$ , an explicit form for a vector potential of a static, homogeneous magnetic field may be written out as

$$\mathbf{A}_0(\mathbf{r}) = \frac{1}{2}\mathbf{B} \times (\mathbf{r} - \mathbf{O}), \quad (1)$$

where  $\mathbf{O}$  is the arbitrarily chosen gauge origin of the system and  $\mathbf{r}$  is the position vector of any point in space. The dependency of

the magnetic vector potential on the arbitrary gauge origin can lead to unphysical contributions to observable quantities, which must be carefully avoided.

The fundamental equation governing the dynamics of molecules in finite magnetic fields is the non-relativistic time-dependent Schrödinger equation (in atomic units),

$$\hat{H}|\Psi\rangle = i\frac{\partial}{\partial t}|\Psi\rangle, \quad (2)$$

where  $\hat{H} = \hat{T}_n + \hat{H}_{\text{el}} + \hat{V}_{\text{nn}}$  is the molecular Hamiltonian operator consisting of the nuclear kinetic energy operator ( $\hat{T}_n$ ), the electronic Hamiltonian operator ( $\hat{H}_{\text{el}}$ ), and the nuclear repulsion potential operator ( $\hat{V}_{\text{nn}}$ ). Since even a strong magnetic field does not change the fact that the motions of the nuclei and the electrons, respectively, occur on completely different time scales, we use the Born–Oppenheimer (BO) ansatz to approximate the wave function,

$$\Psi(\mathbf{r}, \mathbf{R}, t) \approx \varphi(\mathbf{r}, \mathbf{R})\phi(\mathbf{R}, t), \quad (3)$$

with  $\mathbf{R}$  and  $\mathbf{r}$  denoting nuclear and electronic positions, respectively. As a consequence, two coupled equations of motions, the electronic and nuclear Schrödinger equations, can be formulated as

$$\hat{H}_{\text{el}}|\varphi\rangle = i\frac{\partial}{\partial t}|\varphi\rangle, \quad (4)$$

$$\hat{H}_n|\phi\rangle = i\frac{\partial}{\partial t}|\phi\rangle. \quad (5)$$

Assuming that the nuclei can be regarded as classical particles and that the electronic Schrödinger equation only depends parametrically on their position, a potential energy surface (PES),

$$U_{\text{BO}}(\mathbf{R}) = \langle \varphi | \hat{H}_{\text{el}}(\mathbf{R}) | \varphi \rangle, \quad (6)$$

may be calculated for any set of fixed nuclear coordinates by solving the electronic Schrödinger equation. In order to avoid gauge-origin dependencies of  $U_{\text{BO}}$ , London atomic orbitals<sup>37,38</sup> have to be used consistently throughout its construction.<sup>4,5,39</sup> Gradients of the PES may also be constructed in a similar fashion, employing LAOs in order to eliminate gauge-origin dependencies.<sup>6,18</sup> The PES can be constructed at any level of quantum-chemical theory, although it is preferable to use size-consistent methods in order to avoid internal inconsistencies.

### B. Nuclear motion in external magnetic fields

In order to solve the time-dependent nuclear Schrödinger equation (5), it is necessary to construct the effective nuclear Hamiltonian,

$$\hat{H}_n = \hat{T}_n + \hat{V}_n. \quad (7)$$

The nuclear kinetic energy operator  $\hat{T}_n$  can be written as

$$\hat{T}_n = \sum_{I=1}^{N_n} \frac{1}{2M_I} \hat{\Pi}_I^2, \quad (8)$$

$$\hat{\Pi}_I = \mathbf{P}_I - Z_I \mathbf{A}(\mathbf{R}_I) + \chi_I, \quad (9)$$

consisting of the canonical momentum operator  $\mathbf{P}_I = -i\nabla_{\mathbf{R}_I}$ , a contribution from the magnetic vector potential, and the geometric vector potential  $\chi_I = \langle \varphi | \mathbf{P}_I | \varphi \rangle$ , which is also referred to as the Berry connection or Berry potential.<sup>34,35,40</sup>

The nuclear potential energy operator  $\hat{V}_n$ , on the other hand, can be constructed as

$$\hat{V}_n = U_{\text{BO}} + \sum_{I=1}^{N_n} \frac{1}{2M_I} \hat{\Delta}_I + \hat{V}_{\text{nn}}, \quad (10)$$

$$\hat{\Delta}_I = \Delta_I - \chi_I^2, \quad (11)$$

$$\Delta_I = \langle \varphi | \mathbf{P}_I^2 | \varphi \rangle, \quad (12)$$

which consists of the BO potential energy, a nonadiabatic correction also often referred to as the diagonal Born–Oppenheimer correction, and the nuclear repulsion potential. Using assumptions about the locality of all relevant potentials, as well as the definition of the Berry curvature tensor,<sup>34,35</sup>

$$\Omega_{IJ} = \nabla_I \chi_J - \nabla_J \chi_I, \quad (13)$$

the construction of the nuclear equations of motion within a magnetic field becomes relatively straightforward and yields

$$M_I \ddot{\mathbf{R}}_I = -\frac{\partial U_{\text{BO}}(\mathbf{R})}{\partial \mathbf{R}_I} - Z_I \mathbf{B} \times \dot{\mathbf{R}}_I + \sum_J \Omega_{IJ} \dot{\mathbf{R}}_J. \quad (14)$$

This equation of motion can be interpreted as the coupled movements of charged particles within an external magnetic field  $\mathbf{B}$  and within an external potential. As such, the first term in Eq. (14) represents the force of the potential generated by the BO PES, that is, the intramolecular interactions. The second term constitutes the Lorentz force of the external magnetic field on the moving charged particle, that is, the nucleus. The third and last term represents the force generated by the interaction with the screened charges of all other nuclei in the molecule. It should be noted that if all quantities in Eq. (14) are constructed using LAOs, the equation of motion itself becomes gauge-origin independent as well.

The Berry curvature tensor as defined in Eq. (13) contains the nuclear momentum operator working on the electronic wave function. Its computation, thus, involves either solving the coupled-perturbed Hartree–Fock (CPHF) equations<sup>36</sup> or a phase-corrected numerical differentiation scheme.<sup>34</sup> The latter will be used throughout this work.

### C. Solution to the nuclear equation of motion

Because the analytical solution to the differential Eq. (14) is generally not accessible, a numerical integration scheme must be employed. For field free dynamics, it is common to use a symplectic integration scheme like the often discussed velocity-Verlet propagator<sup>41</sup> or propagators of higher order like Runge–Kutta<sup>42</sup> or Forest–Ruth.<sup>43</sup> However, the presence of the Lorentz force and Berry curvature in the equation of motion does not allow for a separation into a pure coordinate propagation step and a pure velocity propagation step while simultaneously maintaining symplecticity.<sup>44</sup>

Tao was able to solve this problem by introducing an auxiliary Hamiltonian that couples to the original through an empirical coupling constant. Peters and co-workers adapted this propagation for MD simulations in magnetic fields.<sup>35,45</sup> However, in order to propagate the molecule one step in time, the auxiliary coordinates and momenta (ACM) propagator requires three gradient calculations, making it three times more expensive than the regular Verlet algorithm. In addition, an empirical coupling constant  $\omega$  must be optimized for every molecule and the intended initial conditions.

In this section, we present an alternative integration scheme that is directly derived from the nuclear equation of motion in Eq. (14). Using the matrix representation  $\hat{\mathbf{B}}$  for the cross product of the Lorentz force in Eq. (14), it can be rewritten in terms of the more compact matrix equation,

$$\mathbf{M}\ddot{\mathbf{R}}(t) = -\nabla U_{\text{BO}}(\mathbf{R}(t)) - \mathbf{Q}(t)\dot{\mathbf{R}}(t), \quad (15)$$

where  $\mathbf{M}$  denotes a diagonal matrix containing the atomic masses.  $\mathbf{R}$  is a vector consisting of the nuclear coordinates constituting the PES, namely,  $\mathbf{R} = (\mathbf{R}_1, \mathbf{R}_2, \dots)^T$ , whereas  $\mathbf{Q}(t)$  is defined as

$$\mathbf{Q}_{IJ}(t) = \delta_{IJ} Z_I \hat{\mathbf{B}} - \Omega_{IJ}, \quad (16)$$

where the quantity  $\hat{B}_{\alpha\beta} = -\epsilon_{\alpha\beta\gamma} B_\gamma$  is the matrix representation for the cross product with the magnetic field and  $\epsilon_{\alpha\beta\gamma}$  is the Levi–Civita symbol.

A pragmatic numerical solution to Eq. (15) was presented by Tajima for a similar problem.<sup>46</sup> By inserting the numerical derivative for  $\dot{\mathbf{R}}(t)$  and the time average for  $\mathbf{R}(t)$  and assuming that the changes in the time dependent potentials  $\Omega(\mathbf{R}(t))$  as well as  $U_{\text{BO}}(\mathbf{R}(t))$  are only small during a propagation step, only the zeroth-order term from a Taylor series needs to be kept

$$\ddot{\mathbf{R}}(t) \approx (\dot{\mathbf{R}}(\tau^+) - \dot{\mathbf{R}}(\tau^-))/\Delta\tau, \quad (17a)$$

$$\dot{\mathbf{R}}(t) \approx (\dot{\mathbf{R}}(\tau^+) + \dot{\mathbf{R}}(\tau^-))/2, \quad (17b)$$

$$\mathbf{Q}(\mathbf{R}(t)) \approx \mathbf{Q}(\tau), \quad (17c)$$

$$U_{\text{BO}}(\mathbf{R}(t)) \approx U_{\text{BO}}(\tau). \quad (17d)$$

Here, the notation  $\mathbf{R}(\tau^\pm) = \mathbf{R}(\tau \pm \Delta\tau/2)$  was used. Inserting Eq. (17) into Eq. (15) and rearranging for  $\dot{\mathbf{R}}(\tau^\pm)$  lead to an expression for the updated velocities,

$$\begin{aligned} \dot{\mathbf{R}}(\tau^+) = & -\Delta\tau \left( \mathbf{I} - \frac{\Delta\tau}{2} \mathbf{Q}(\tau) \right)^{-1} \nabla U_{\text{BO}}(\tau) \\ & + \left( \mathbf{I} - \frac{\Delta\tau}{2} \mathbf{Q}(\tau) \right)^{-1} \left( \mathbf{I} + \frac{\Delta\tau}{2} \mathbf{Q}(\tau) \right) \dot{\mathbf{R}}(\tau^-). \end{aligned} \quad (18)$$

After updating the velocities, the coordinate propagation can simply be computed as

$$\mathbf{R}(\tau + \Delta\tau) = \mathbf{R}(\tau) + \Delta\tau \dot{\mathbf{R}}(\tau^+). \quad (19)$$

It should be noted that, in the limit of  $|\mathbf{B}| \rightarrow 0$ ,  $\mathbf{Q}$  vanishes and the velocity-Verlet propagation is obtained. There are several advantages of the Tajima approach compared to using the ACM propagator. Mainly, one propagation step  $\Delta\tau$  requires only a single gradient and Berry curvature calculation. In addition, both the auxiliary coordinates and momenta, as well as the empirical coupling constant, can be dropped. The Tajima propagator is, thus, both more compact and efficient than the ACM propagator. This is especially advantageous for on-the-fly simulations where the molecular gradients and the Berry curvature have to be calculated *ab initio* during every propagation step.

Finally, we would like to note that the computational cost and numerical stability of the matrix inversion needed in the framework of the Tajima approach are not issues for the very small molecules studied in this work. This may become more important when treating very large molecular systems.

### III. COMPUTATIONAL DETAILS

#### A. Quantum-chemical calculation of molecular properties

All relevant molecular properties have been calculated using the TURBOMOLE<sup>47–49</sup> package. A gauge origin invariant implementation of the generalized Hartree–Fock (GHF) method into the TURBOMOLE package was presented by Pausch and Klopper in 2020.<sup>50,51</sup> For this work, extensions to molecular GHF gradients and the MP2 method in finite magnetic fields have been implemented into the TURBOMOLE package consistent with recent publications.<sup>18,52</sup> Our MP2 implementation was based on the two-component MP2 approach implemented into the RIC2 module of the TURBOMOLE package and differs only in the employment of LAOs.<sup>53,54</sup> Throughout this work, a def2-TZVP basis set<sup>55,56</sup> was used for all calculations. The resolution-of-the-identity (RI) approximation was used for the calculation of MP2 energies using the corresponding def2-TZVP auxiliary basis set.<sup>57</sup>

#### B. Spline fitting

To reduce the computation time, a two-dimensional scan along the bond distance  $d$  and relative angle to the magnetic field  $\theta$  was pre-calculated in order to store all necessary quantities

for the nuclear propagation on disk (nuclear gradients and Berry curvature). Moreover, any observable quantity can also be pre-calculated and stored on a disk if needed. For instance, it is helpful to examine if the energy is properly conserved, which requires the electronic energy to be stored. Furthermore, electric dipole moments are needed in order to obtain infrared spectra. It should be noted that any observable quantity should be calculated using LAOs to maintain gauge origin invariance.

All relevant quantities are then fitted by calculating root points on a fine meshed grid and the corresponding partial second derivatives are estimated so that a bivalent spline function can be created during the simulation. This procedure was already presented in an earlier publication,<sup>35</sup> where the molecular gradients and Berry curvature were obtained as derivatives of the electronic energy and wave function.

However, since the PES is already approximated via a spline, there really is no need to pre-compute the molecular gradients and use a spline fit for them as well, as they can simply be computed as derivatives of the PES spline during the simulation. We have compared the two approaches (pre-calculated analytical molecular gradients vs gradients of the PES spline) and have found no discernible differences in the results.

In addition, such an approach allows us to take correlation effects into account while the gradients are automatically obtained at the same level of theory. In this work, all correlated calculations are performed at the two-component MP2 level. It should be noted that the first derivatives of the PES spline have to be calculated for both dimensions of the PES ( $d$  and  $\theta$ ). The Berry curvature tensor is calculated at the GHF level and each of its elements must be fitted separately through a spline function.

All pre-calculations for this work have been carried out at the GHF/def2-TZVP and MP2/def2-TZVP levels of theory using the TURBOMOLE program package while using a convergence criterion of  $10^{-11} E_h$ . For the spline functions, a  $99 \times 99$  grid was precalculated with a step size of  $\Delta d = 0.012a_0$  and  $\Delta\theta = \pi/98$  for the  $\text{H}_2$  molecule and  $\Delta d = 0.035a_0$  and  $\Delta\theta = \pi/98$  for the LiH molecule. The minimum and maximum bond distances for the  $\text{H}_2$  molecule were chosen to be  $0.6a_0$  and  $1.8a_0$  and for the LiH molecule  $0.5a_0$  and  $4.0a_0$ , respectively.

#### C. Performance of the Tajima propagator

Figure 1 shows the standard deviation of the Tajima and ACM propagators for the  $\text{H}_2$  molecule within a 20 ps long simulation. The ACM propagator was used in a velocity-Verlet propagation scheme, where the coupling constant  $\omega$  was optimized for a field of  $0.1B_0$  using the smallest step size 0.024 fs. Both algorithms were initiated from the equilibrium geometry with an initial kinetic energy of  $0.02E_h$ , while the center-of-mass motion was suppressed in the initial step.

The Tajima propagator performs significantly better than the ACM propagator throughout all simulations while simultaneously being three times faster. Note that by adjusting the coupling constant  $\omega$ , the performance of the ACM propagator could be significantly improved, and in principle, a similar standard deviation as that of the Tajima propagator could be achieved. In addition to the total energy, the regular pseudo-momentum as defined in Ref. 35 was recorded as a second conserved quantity in an external magnetic field.



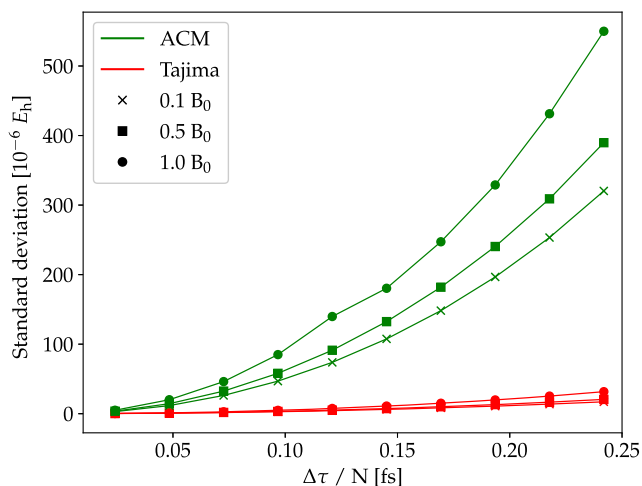


**FIG. 1.** Influence of the step size  $\Delta\tau$  and field strength  $|B|$  on the stability of the dynamics of  $H_2$  for the ACM and Tajima propagators. The time step  $\Delta\tau$  is divided by  $N = 3$  for the Tajima propagator to yield the same computational cost. The coupling constant  $\omega$  for the ACM propagator was adjusted for the smallest step size ( $\omega = 1.5$ ).

However, since the change in the total pseudo-momentum was negligible ( $<10^{-13} \hbar/a_0$ ) in all simulations, it is not further considered in this work.

#### IV. $H_2$ MOLECULE

The influence of an external magnetic field on the molecular rotations and vibrations of the  $H_2$  molecule can mostly be separated into two different parts. First is the influence of the magnetic field on the electronic wave function through paramagnetic and diamagnetic contributions as presented in Eq. (4). This, of course,

affects the BO potential energy surface  $U_{BO}$ , leading to an altered PES, which additionally depends on the orientation of the molecule with respect to the external field. Second, since during molecular rotations and vibrations, the atomic nuclei can essentially be considered as moving charges, an external magnetic field interacts with them through a Lorentz force. However, it can be assumed that the electrons screen the positively charged nuclei to some extent, meaning that only a portion of the Lorentz force that would interact with the bare nuclei will actually have an impact. This effective screening is considered through the Berry curvature tensor as shown in Eq. (16).

Both of these considerations have been introduced as well as discussed in an earlier publication.<sup>35</sup> However, we believe that it is important to carefully assess them once more, particularly in order to capture some effects that have not yet been covered. In addition, correlation effects should be taken into account by employing a PES generated by the MP2 level of theory, leading to small shifts in the vibrational and rotational spectra. A magnetic field applied parallel to the  $z$  axis is assumed throughout this section.

#### A. Changes to the potential energy surface

In the absence of an external field, the PES of the  $H_2$  molecule depends only on one internal coordinate: the bond distance  $d$ . Under the influence of a magnetic field, however, the system is no longer rotationally invariant, and thus, the polar angle between the field and the molecular bond,  $\theta$ , has to be considered as well. A two-dimensional contour plot of the potential energy surface in a magnetic field of  $B = 0.4B_0$  is shown in Fig. 2(a). The most apparent change caused by the magnetic field is the molecule's preferred parallel orientation relative to the field and the resulting potential barrier for a perpendicular orientation. Since the height of the  $\cos^2(\theta)$ -like potential is almost proportional to the magnetic field strength, it is reasonable to assume that its effects also scale linearly with respect to the field strength. A far less prevalent but still noticeable effect of the magnetic field on the PES is the dependency of the equilibrium bond length on the orientation of the molecule with

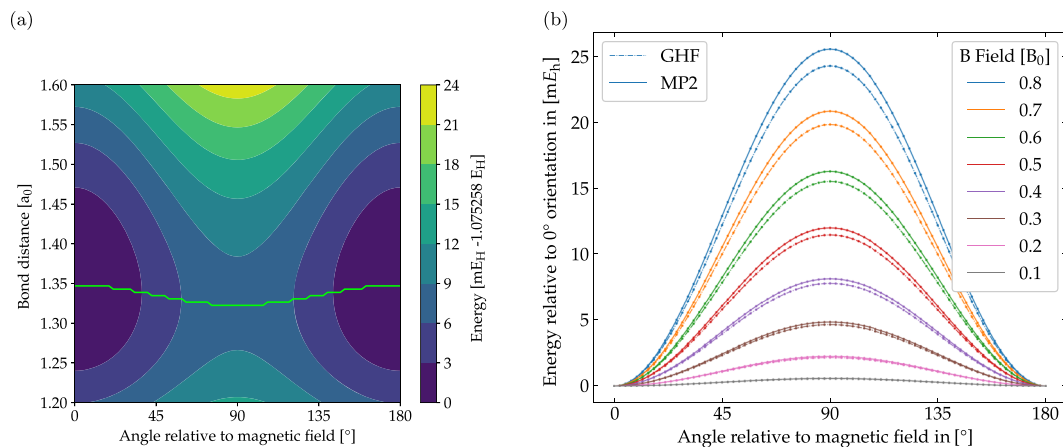


**FIG. 2.** (a) Potential energy surface of  $H_2$  for  $B_z = 0.4B_0$ . The green line indicates the corresponding equilibrium bond distance. The calculation was carried out with a def2-TVZP basis set at the MP2 level. (b) Cosine-like potential for the equilibrium bond length plotted against the angle, relative to the fields of different strengths.

respect to the field. However, compared to the previously discussed potential energy barrier, this effect turns out to be comparably small.

Before studying the dynamics of  $\text{H}_2$  in detail, a qualitative assessment of the expected influence of such a potential barrier should be discussed. Since the system's total energy has to be conserved, the kinetic energy is reduced every time the molecule is near the perpendicular orientation, resulting in a hindered rotation of the molecule. Moreover, if the potential energy barrier is large enough (i.e., in extremely strong magnetic fields), the kinetic energy reduces to almost zero and a rotation of the molecule over the barrier is no longer possible. Such a trajectory is called a libration. Since all assumptions about the molecular rotation behaving like a free rigid rotor fail under such conditions, a sudden shift in the rotational spectrum at a certain magnetic field strength is to be expected.

The correlation effects on the potential energy barrier should also be assessed. In Fig. 2(b), the potential energy barrier is plotted for different field strengths using both the GHF and the MP2 methods. While the correlation effects appear to be small, it should be noted that they become more pronounced with an increasing field strength.

## B. Trajectory of a molecular rotation

The distinction between the trajectories of an (allowed but hindered) rotation and a libration is depicted in Fig. 3. Both trajectories were simulated in an external field of  $0.2B_0$ , but slightly different initial velocities were chosen. For the first simulation shown in Fig. 3(a), the molecule was given an initial kinetic energy of  $3.5 mE_h$ , which is just enough to ensure that the potential energy barrier is crossed, resulting in a rotation. For the second simulation shown in Fig. 3(b), the simulation was started with a kinetic energy of  $2.8 mE_h$ , which is not sufficient to overcome the potential energy barrier. In both cases, some energy was also put into a stretching vibration that couples with the rotation and libration, respectively, while any center-of-mass motion was suppressed.

The trajectories in Fig. 3 also reveal the main influence of the Lorentz force interacting with the nuclear velocities: a slow rotation of the molecule about the field axis. It should be noted that the corresponding simulations were initiated from the equilibrium orientation parallel to the field with no initial angular velocity around the field axis. Thus, according to the principle of conservation of angular momentum, such a rotation can only be caused by an external force, which, in this case, corresponds to the Lorentz force acting on the (partially screened) nuclei. We refer to this motion as Lorentz-force induced precession of the rotational axis. This precession has to be carefully distinguished from center-of-mass cyclotron rotations of charged systems like the  $\text{H}_2^+$  molecule. In such cases, the Lorentz force would initiate a regular cyclotron rotation of the entire molecule about a fixed point in space, whereas the Lorentz-force induced precession does not correspond to an overall movement of the center-of-mass of the molecule in space.

By performing a large number of MD simulations on the  $\text{H}_2$  molecule, we have assessed the two main effects of an external magnetic field on molecular rotations and vibrations. On the one hand, we have to consider an additional potential barrier arising from a dependency of the PES on the orientation between the molecule and the magnetic field. On the other hand, Lorentz forces will interact with the screened atomic nuclei, leading to additional movements. While most of this work is, therefore, focusing on these two effects, it should be noted that the MD simulations also take into account other effects. First, as already mentioned, the equilibrium bond distance depends on the orientation of the molecule with respect to the external field. Thus, it is likely to change during a molecular rotation, inducing stretching vibrations that are coupled to the respective rotations. Second, the reversed case is also relevant, as stretching vibrations can induce rotations at a very low frequency. This was shown previously by Ceresoli *et al.*<sup>33</sup> Third, coupling effects from field-free dynamics, such as centrifugal lengthening, also occur in a magnetic field. However, these effects are not the subject of detailed analysis in this work.

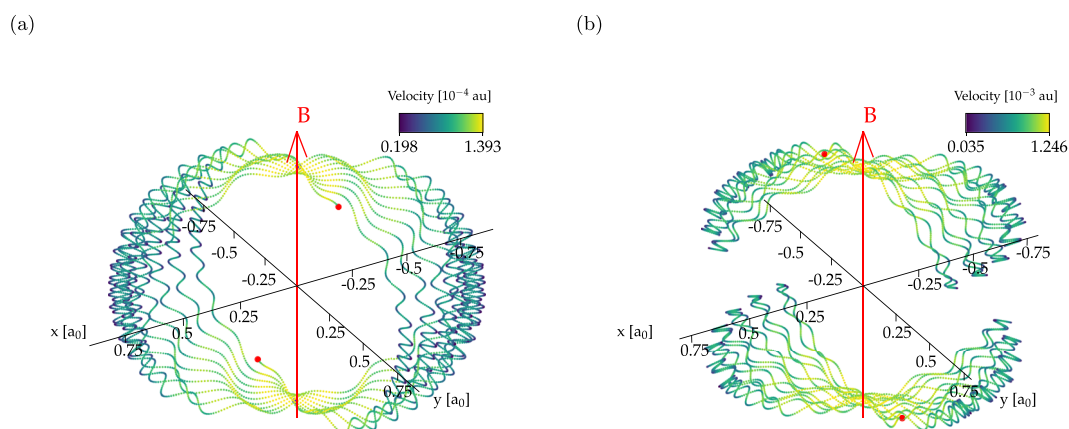


**FIG. 3.** Trajectory for the  $\text{H}_2$  molecule in a magnetic field of  $B_z = 0.2B_0$ . The hindered rotation (a) was initiated with  $3.5 mE_h$  and the libration (b) with  $2.8 mE_h$ . The nuclear velocity is indicated by different color shades. A darker color corresponds to a slower rotation. For the depicted total simulation time of 435 fs, the molecule rotates  $90^\circ$  about the magnetic field axis.

### C. Generating rotational and vibrational spectra

After having assessed molecular rotations and librations qualitatively in Sec. IV B, it is time to analyze them quantitatively as well. A power spectrum can be obtained by recording the nuclear velocities from an MD simulation and subsequently performing a Fourier transformation.<sup>58–60</sup> In general, such a spectrum can be regarded as a vibrational spectrum *without selection rules* so that the obtained intensities reflect how often a mode occurred during the simulation instead of spectroscopic intensities.

To get a better picture of the two major effects that the external magnetic field has on the molecular rotations or librations, it is helpful to study the influence of the potential barrier and the Lorentz forces separately. This can easily be done by first carrying out a simulation while neglecting the Lorentz force and Berry curvature in Eq. (14), which corresponds to a physical picture where the nuclear charges are fully screened by the electrons. A subsequent simulation where both the Lorentz force and the Berry curvature are taken fully into account is then carried out in order to study their effects as well. For the simulations in this discussion, the same initial conditions shown for the trajectories in Fig. 3 were chosen. The resulting spectrum is presented in Fig. 4.

It is now possible to analyze the influence of the potential energy barrier on the spectrum by neglecting the Lorentz force and the Berry curvature in Eq. (14) during the simulation. The most noticeable change in the spectrum is that, because of the anharmonic shape of the potential energy barrier, rotational overtones become visible that would otherwise not appear in the spectrum of the field-free case. While these overtones can be observed for both rotations and librations, they differ fundamentally in these two cases. For a rotation, overtones will appear at every odd multiple of the fundamental frequency, while even multiples are unoccupied. Carrying out a Fourier transformation for each Cartesian component  $(x, y, z)$  separately reveals a great deal about the symmetry of these frequencies. They are aligned in a pattern that can be described by the following notation:

$$(x, y, z)^{\text{rot}} \rightarrow \underline{(x, y, z)}, \emptyset, (x, y, z), \emptyset, \dots$$

In this notation, the fundamental oscillation (rotation, libration, and stretching vibration) is written to the left and denotes the union of all frequencies occurring in the corresponding fine structure, which can be found on the right hand side of the arrow. A singular peak is represented by a bracket with the associated designation of symmetry. The frequencies appear in ascending order from left to right. The notation  $\emptyset$  is used for an unoccupied frequency, and the fundamental frequency is underlined.

An entirely different case presents itself for librations. As shown in the spectrum, every multiple of the fundamental frequency is occupied with an overtone. Moreover, an analysis of the different Cartesian components reveals that the fundamental frequency is only active in the  $(x, y)$  component and that overtones alternate between  $(z)$  and  $(x, y)$  symmetry. Thus, peaks of  $(z)$  symmetry occupy the even multiples of the fundamental frequency, while peaks of  $(x, y)$  symmetry are found at the odd positions,

$$(x, y, z)^{\text{lib}} \rightarrow \underline{(x, y)}, (z), (x, y), (z), \dots$$

A similar pattern presents itself for the stretching vibration, which, as mentioned before, couples directly to all rotational or librational motions. In a field-free spectrum, this would lead to characteristic P- and R-branches to the left and right of the fundamental vibrational frequency. The presence of additional rotational overtones, however, gives rise to a complex coupling pattern, where each vibrational mode is coupled to all rotational modes. A single vibrational peak, therefore, leads to a multiplet mirroring the rotational spectrum. Moreover, if the magnetic field strength is large enough to induce molecular librations, an additional mode corresponding to  $(z)$  symmetry remains uncoupled from the stretching vibration (Q-branch). This situation can be summarized in the following patterns:

$$(x, y, z)^{\text{str}}_{\text{rot}} \rightarrow \dots, \emptyset, (x, y, z), \underline{(z)}, (x, y, z), \emptyset, \dots$$

$$(x, y, z)^{\text{str}}_{\text{lib}} \rightarrow \dots, (z), (x, y), \underline{(z)}, (x, y), (z), \dots$$

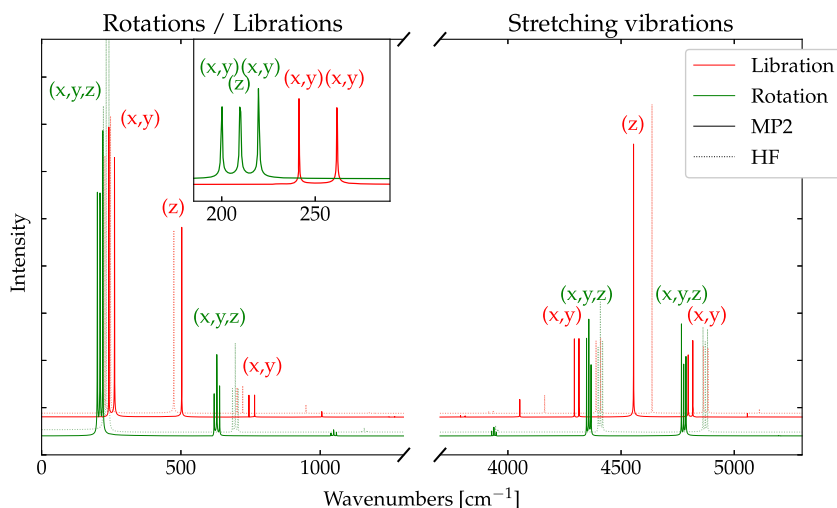


**FIG. 4.** Spectrum for the  $\text{H}_2$  molecule in a magnetic field of  $0.2B_0$ . The initial conditions were chosen to be equivalent to the trajectories in Fig. 3. The molecule was simulated for a timespan of 20 ps.



In Sec. IV B, the precession of the axis of rotation was introduced. This precession is an effect of the Lorentz force and Berry curvature, and as such, it is not visible in trajectories or spectra where these terms are neglected. If all terms are fully taken into account, then the modes corresponding to the precession occur naturally in the respective spectrum.

Two main conclusions can be drawn from the spectra where these effects are included. First, since the frequency of such a rotation is relatively low, their contribution to the spectrum is usually small. Second, since Lorentz forces are applied perpendicular to the external magnetic field along the ( $z$ ) axis, precessions can only couple to motions in the ( $x$ ) and ( $y$ ) components, while motions parallel to the ( $z$ ) axis remain unaffected. As a consequence, frequencies of ( $x, y$ ) symmetry are split into doublets, with a coupling constant equal to twice the frequency of the precession.

For a rotation, this yields a ( $x, y$ ) $^{\pm}$  doublet, where the  $\pm$  notation indicates the splitting, and an uncoupled ( $z$ ) singlet,

$$(x, y, z)^{\text{rot}} \rightarrow \underline{(x, y, z)^{\pm}}, \emptyset, (x, y, z)^{\pm}, \emptyset, \dots,$$

and similarly, for a libration,

$$(x, y, z)^{\text{lib}} \rightarrow \underline{(x, y)^{\pm}}, (z), (x, y)^{\pm}, (z), \dots$$

This coupling pattern works also for stretching vibrations. It should be noted that the frequency of the Lorentz-force induced precession itself does not appear in the spectrum and becomes visible only through couplings in the ( $x, y$ ) components of the rotation or libration.

Moving on to the contribution of electron correlation on the rotational and vibrational spectra of  $\text{H}_2$  in a strong magnetic field, it is helpful to analyze the differences between a simulation on a GHF PES and on an MP2 PES, which is also found in Fig. 4. As mentioned before, MP2 calculations lead to slightly higher potential energy barriers than do their GHF counterparts [Fig. 2(b)] and, as a consequence, rotations are slightly more hindered and shifted to the red. For librations, on the other hand, a higher potential energy barrier means that the molecule loses kinetic energy faster, reaching the maximum amplitude of its libration sooner. Frequencies of a libration are, therefore, blue-shifted. This effect can be observed particularly well for overtones since the shifts of the fundamental frequencies are multiplied there as well. Finally, stretching vibrations are shifted to lower frequencies, presumably due to a less sharp potential with respect to the bond distance. Qualitatively, however, GHF and MP2 PESs produce the same results. Note that, by also calculating the Berry curvature at the MP2 level of theory, the differences might be larger.

One very important contribution to the rotational and vibrational spectra has been neglected up until now. So far, only those trajectories and spectra were shown and discussed that were generated from initial conditions corresponding to a parallel orientation of the molecule with respect to the external field, that is, the equilibrium conformation. In principle, while any conformation on the PES could be used as the initial geometry and for molecules in field-free simulations, it is generally assumed that the equilibrium geometry is a good starting point.

For  $\text{H}_2$  in a strong magnetic field, however, this equilibrium orientation is a special point on the PES for two reasons. First, at equilibrium, no initial energy can be put into the precession around the ( $z$ ) axis, meaning that the entire initial nuclear kinetic energy is put into rotations pointing toward the potential energy barrier. As a consequence, the potential energy barrier can be overcome relatively easily, which is not at all representative of the system in general. These initial conditions, thus, favor rotations over librations. Second, the splitting of the ( $x, y$ ) $^{\pm}$  components presented so far could be taken to imply that their coupling is constant, but this is only true for simulations started from the parallel-field orientation since no initial rotation about the field axis can be excited. By choosing a different starting geometry, an initial energy can also be added to these rotations, leading to different coupling constants.

Since simulations started from the equilibrium orientation are, thus, not necessarily representative of the ensemble, they should be viewed with some caution. Different initial conditions and especially different initial orientations can change the spectrum quite significantly. Nevertheless, simulations started from the equilibrium orientation will exhibit all effects induced by an external magnetic field and, as such, they are a good starting point for a qualitative assessment of rotational and vibrational spectra of  $\text{H}_2$  in a strong magnetic field.

#### D. Impact of field strength on the spectrum

Having discussed the general changes of rotational spectra in external magnetic fields, the next step will be an investigation of how those changes occur depending on the magnetic field strength. For this, a set of 200 spectra were calculated for field strengths between  $0B_0$  and  $2B_0$  while keeping the initial velocity fixed for all simulations. By plotting all peaks with an intensity above a given threshold against the magnetic field strength, it is possible to observe how the spectrum changes gradually. This is depicted in Fig. 5. The

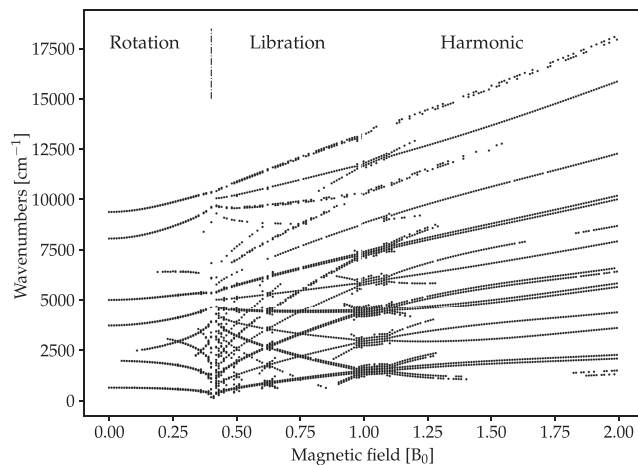


**FIG. 5.** Peaks with highest intensities collected from 200  $\text{H}_2$  spectra as a function of the magnetic field strength. The field has been changed with an increment of  $0.01B_0$ . To create a single spectrum, a step size of  $\Delta t = 0.072$  fs and a total simulation time of 70 ps were chosen.

equilibrium orientation was chosen as a starting point for all spectra as it correctly reproduces all effects that are investigated here. It should, however, be stressed that other initial conditions would lead to different spectra.

Starting from the zero-field case and going up to higher magnetic field strengths, this section's aim is a quantitative assessment of a rovibrational spectrum as a function of the field strength. It should be noted that the graph in Fig. 5 is not sensitive to the intensities of the peaks. Often, different intensities can differ by a factor of up to  $10^3$ , for instance, a stretching vibration and its first harmonic. Nevertheless, it can be fruitful to track even small peaks in order to capture all effects of the magnetic field on the spectrum. It is, however, necessary to be able to differentiate between very small peaks and background noise, which is why a threshold intensity needs to be defined. Every signal with an intensity greater than the threshold is considered to be a peak. For very small peaks with intensities close to the threshold, it is, thus, possible that they are visible at a certain field strength but not at another one. This does not imply that a peak vanishes, just that its intensity dropped below the arbitrarily but carefully chosen threshold.

### 1. $0.0B_0$

A total number of five peaks are distinctly visible in the field-free spectrum. The lower peak with a frequency of  $680\text{ cm}^{-1}$  can be assigned to the rotational mode. Both of the next peaks with frequencies at  $3760$  and  $5170\text{ cm}^{-1}$  belong to the fundamental frequency of the stretching vibration, which is split into P- and R-branches since they couple with the rotational mode. The highest two frequencies ( $8250$  and  $9600\text{ cm}^{-1}$ ) can be assigned to the first harmonic of the stretching vibration, which again forms P- and R-branches.

### 2. $0.1B_0$

The influence of the magnetic field on the electronic structure is no longer negligible and the potential energy barrier perpendicular to the field axis leads to an anharmonic potential. Consequently, the second rotational overtones start to appear in the spectrum. As expected for a rotation, only uneven multiples of the fundamental frequency appear in the spectrum, so the first overtone is missing. Furthermore, the nuclear velocities interact with the magnetic field and a precession around the field axis ( $z$ ) is induced. This precession couples to all frequencies assigned to the  $(x, y)$  components of the rotational modes, and hence, they are split into doublets, while peaks belonging to the  $(z)$  component remain unaffected. As mentioned before, the isolated frequency of the precession never appears in any of the spectra and can only be observed through the couplings to other rotational modes.

### 3. $0.1-0.4B_0$

The height of the potential energy barrier increases and slows down the rotational movement. As a consequence, all frequencies corresponding to the rotation are red-shifted. In addition, even more overtones become visible. Also, as the intensities of the overtones increase, the coupled rotational overtones of the stretching vibrations start to become more significant. Therefore, more peaks belonging to the P- and R-branches can be seen in the spectrum.

### 4. $0.4B_0$

At this field strength, the most radical change in the spectrum takes place. As the potential energy barrier becomes even higher, the initial kinetic energy is no longer large enough for a rotation to take place. At this point, the calculated trajectory alternates between very slow rotations and a libration, which is why no evaluable spectrum can be obtained from it. This might be fixed by choosing a longer simulation time. The transition from the rotational case to the librational one can be seen clearly in Fig. 5. The most noticeable changes in the spectrum are the shifted frequencies belonging to the  $(z)$  component of the modes that now appear at even multiples of the fundamental frequency. Furthermore, the stretching vibration and its first harmonic now not only exhibit P- and R-branches but also a Q-branch belonging to the uncoupled vibrational frequency of  $(z)$  symmetry.

### 5. $0.4-1.5B_0$

As expected, the frequencies of librations are blue-shifted because the potential energy barrier increases even further with the field strength. A similar blue-shift can also be obtained for the Q- and R-branches of the stretching vibration due to a sharper potential in the bond distance. The P-branch, on the other hand, is red-shifted because the corresponding libration frequencies with which the P-branch couples show a stronger blue-shift than the Q-branch. In this region, three particular field strengths ( $0.56B_0$ ,  $0.67B_0$ , and  $1.2B_0$ ) exhibit unusual behavior. At these points, peaks of modes belonging to the same symmetry cross, leading to a resonance phenomenon where many modes couple in an almost chaotic fashion, creating a multitude of small coupled peaks. For these particular field strengths, librational overtones and coupled stretching vibrations appear at the same frequencies, which implies that the coupling is almost akin to a Fermi resonance. It should be noted that these resonances can only appear for crossings of the same symmetry, for example, an  $(x, y)$  libration crosses a  $(x, y)$  stretching vibration or the same pattern for the  $(z)$  component.

### 6. $1.5B_0$ and higher

The potential energy barrier perpendicular to the field becomes so high that the change in angle relative to the magnetic field axis does not exceed a few degrees. Essentially, the librational movement can be well described by a harmonic approximation, simplifying the spectrum significantly. At a magnetic field strength of  $2B_0$ , the spectrum contains nine equidistant visible frequencies that are separately described through their own fine structure. Furthermore, a strong coupling between librations and stretching vibrations leads to an interconnection between these two phenomena, making them almost indistinguishable. The spectrum is now more akin to that of a harmonic oscillator, which is to be expected as the physical case slowly enters the Landau region.

It should be emphasized once more that all spectra in Fig. 5 were generated from the same initial conditions (parallel orientation to the magnetic field, same nuclear kinetic energy). A different set of initial conditions would lead to completely different spectra, and it is, therefore, necessary to analyze not only one set of initial conditions but the entire ensemble. Especially, the cusp appearing at  $0.4B_0$  would rather be expected at lower field strengths, since, as

already discussed earlier, the equilibrium geometry favors rotations over librations.

### E. Canonical ensemble

In order to obtain results that are independent of a specific set of initial conditions, it is necessary to perform the simulations for an ensemble. For this investigation, we have chosen the canonical ( $N, V, T$ ) ensemble so that integrals of peaks in the ensemble spectrum reflect the number of underlying modes. Note that, according to Ref. 61, this corresponds to a quantum-mechanical spectrum with the discrete rotational bands *smearred out*. At this point, we want to stress again that the power spectrum does not take into account spectroscopic selection rules. To obtain a representative ensemble for the temperature  $T$ , the initial velocities were randomly chosen from a Maxwell–Boltzmann distribution at temperature  $T$ . The subsequent MD simulation was aborted after a suitable time period  $\Delta\tau$  and a spectrum was generated. Then, a new set of initial velocities is drawn while the coordinates from the previous simulation are maintained.<sup>61</sup> Finally, all calculated spectra are averaged, and in order to generate a smoother spectrum, the intensities were averaged over a constant interval of  $\omega \pm 20 \text{ cm}^{-1}$ . A series of spectra generated for a canonical ensemble at 1500 K are shown in Fig. 6 for a subset of different magnetic field strengths.

For the field-free case, one rotational band can be observed, and for the stretching vibration, the corresponding P- and R-branches. If the magnetic field is increased, the first noticeable effect is the appearance of a Q-branch in the stretching vibration, which indicates the presence of librations. However, since the potential energy barrier is still relatively low, rotations are still more likely for this field strength.

Continuing to higher magnetic field strengths, a small red-shift of the entire rotational band becomes visible. This is to be expected for rotations, implying that rotation-like trajectories dominate the ensemble for up to  $0.4B_0$ . For higher field strengths, on the other hand, the entire rotational band starts to be blue-shifted, which is the first indicator for a significantly increased number of librations in the ensemble. In addition, the first overtone of the rotation appears within the spectrum, indicating the anharmonicity of the respective

potential. Both of these findings strongly imply that librations start to become more likely in this region and for higher field strengths.

As mentioned before, librational frequencies are expected to increase linearly with the magnetic field strength, which corresponds directly to the linear dependency between the librational frequency and the height of the potential barrier (see Fig. 2). Corresponding to the higher fundamental frequencies of librations, the coupling between P- and R-branches also becomes stronger. Furthermore, the Q-branch is blue-shifted as well, as the potential for the bond length becomes sharper, too. Finally, for field strengths larger than  $1.6B_0$ , the coupling to the precession becomes visible in the fundamental frequency of the libration, which splits into a doublet.

In summary, all major effects that have been described in Sec. IV A are present in the spectrum of the canonical ensemble. The effect of the magnetic field on a rotational spectrum can, thus, be summarized as an initial red-shift of the frequencies due to a majority of trajectories belonging to rotational movements. If the field strength becomes larger, the frequencies are blue-shifted as librations become more and more important. In addition, the first rotational overtones start to appear. Moreover, in the stretching vibrational spectrum, an additional Q-branch starts to appear, indicating the presence of librations. The frequency of the whole stretching vibration is also blue-shifted due to a sharper potential in the bond distance.

## V. LiH MOLECULE

This section focuses on the rotational and vibrational spectrum of the lithium hydride molecule. Compared to the spectrum of  $\text{H}_2$ , which was presented in great detail in the last section, some significant changes are to be expected here. It is, therefore, necessary to briefly discuss the general properties of LiH and its electronic states.

### A. Properties of LiH in an external field

The external magnetic field pseudovector reduces the symmetry of LiH. While its molecular point group is  $C_{\infty v}$  in the absence

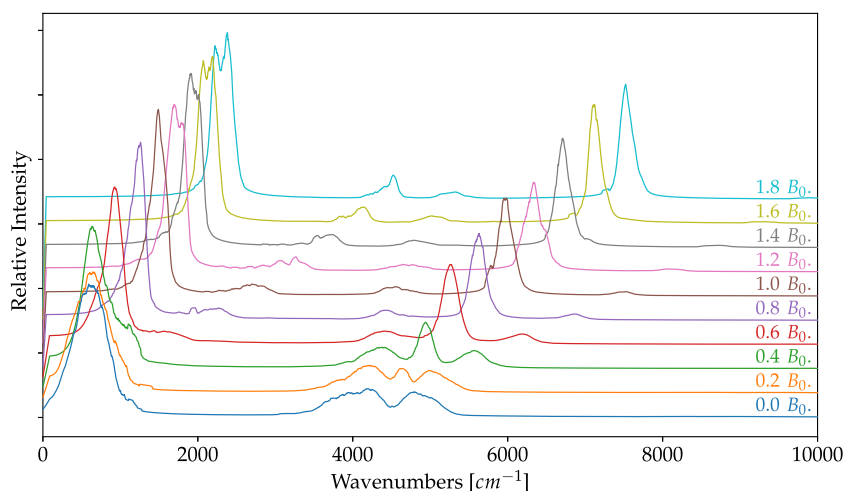


**FIG. 6.** For the canonical ensemble, a set of 2000 spectra were calculated using a target temperature of 1500 K. Every single spectrum was calculated from a 1 ps long simulation using initial velocities from a Maxwell–Boltzmann distribution. To smooth the averaged spectrum, all frequencies were averaged in an interval of  $\omega \pm 20 \text{ cm}^{-1}$ .

of a field, only three possible distinct symmetries are possible within an external magnetic field. If the molecule is oriented parallel to the magnetic field, it possesses  $C_\infty$  symmetry. If it is oriented perpendicular to the external field, its molecular point group is  $C_s$ . For all other cases, the system is  $C_1$ -symmetric.<sup>62,63</sup>

As the LiH molecule possesses a permanent dipole moment that changes with bond length, the vibrational spectrum is active in the infrared (IR) region, and thus, IR spectra of LiH can be obtained.  $H_2$ , on the other hand, is not IR active but possesses a Raman spectrum instead, which directly follows from basic principles of group theory and the rule of mutual exclusion for a molecule with a center of inversion.

The electronic states of LiH have previously been investigated by Stopkowicz *et al.*<sup>10</sup> including electron correlation effects in a magnetic field. We have performed quantum-chemical calculations at the MP2/def2-TZVP level in order to confirm these findings at the level of theory used throughout this section. They are depicted in Fig. 7. While the singlet state ( $^1\Sigma$ ,  $^1A'$ , or  $^1A$  depending on the orientation with respect to the magnetic field) is the most stable at small magnetic field strengths, the spin- and orbital-Zeeman contributions lead to a change in the electronic ground state at about  $0.1B_0$ . Above this field strength, the triplet states ( $^3\Pi$ ,  $^3A'$ , or  $^3A$ ) become more stable. While  $^3\Pi$  and  $^3A'$  are in principle slightly bound, no stable vibrational state can exist within the potential energy wells of these states. Therefore, no vibrational or rotational spectra will exist for these states, and this work is only concerned with singlet states. While these singlet states may be excited states for all magnetic field strengths above  $0.1B_0$ , the general behavior of vibrational and rotational spectra for linear molecules with permanent dipole moments is still captured and, thus, worth investigating.

## B. Changes to the potential energy surface

Comparing the singlet states of LiH and  $H_2$ , one of the most noticeable differences is that the equilibrium orientation of  $H_2$

with respect to the magnetic field is parallel while for LiH the perpendicular orientation is more stable. This can be clearly seen in Figs. 7(b) and 8(a) for a field strength of  $0.2B_0$ . Figure 8(b) also depicts the potential energy barrier as a function of the angle between LiH and the external field for different field strengths.

While a parallel equilibrium orientation ( $H_2$ ) only corresponds to a single conformation, there exists an infinite set of degenerate conformations for the perpendicular orientation (LiH). This is due to the fact that the molecule can be freely rotated around the azimuthal angle  $\phi$ , which is not referenced in Fig. 8(a). The immediate consequence of these different equilibrium conformations for  $H_2$  and LiH becomes apparent by examining the trajectories in Fig. 9. The clear distinction between rotations and librations as discussed for  $H_2$  cannot be made for LiH. While the hydrogen molecule must pass the maximum of the potential energy barrier (an infinite number of points corresponding to a  $360^\circ$  rotation in  $\phi$ ) in order to perform a proper rotation, there is no need for LiH to perform a similar movement. As depicted in Fig. 9(a), LiH will instead have a precession-like movement corresponding to a rotation, and during such a trajectory, the molecule never passes the parallel conformation. Some trajectories may then be more rotation-like [Fig. 9(a)] and some more libration-like [Fig. 9(b)]; however, a clear distinction between these two phenomena cannot be made anymore. With an increasing magnetic field strength, the rotation character of these movements is increasingly lost while they gain more and more libration character. It is more a continuous transition than a tipping point.

## C. Trajectory of a molecular rotation

Exemplary trajectories of molecular rotation-like or libration-like movements are depicted in Fig. 9. In addition to the aforementioned effects, the influence of the Lorentz force on LiH is slightly different from  $H_2$ , where it induces a precession around the magnetic field axis. LiH, however, possesses a permanent dipole moment

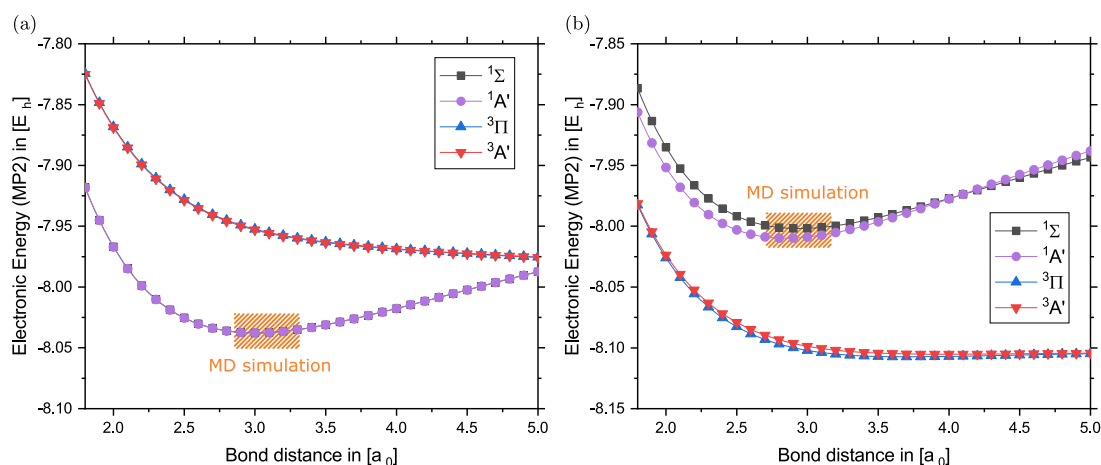


**FIG. 7.** (a) Potential energy surfaces for the parallel and perpendicular orientations of LiH for  $B_z = 0.02B_0$ . Both the singlet ( $^1\Sigma$  and  $^1A'$ ) and the triplet ( $^3\Pi$  and  $^3A'$ ) electronic states are depicted. The relevant area for the MD simulations is marked in orange. (b) Same potential energy surfaces but for  $B_z = 0.2B_0$ . Since the non-binding triplet states are now lower in energy than the singlet states, the MD simulations are run on an excited singlet state.

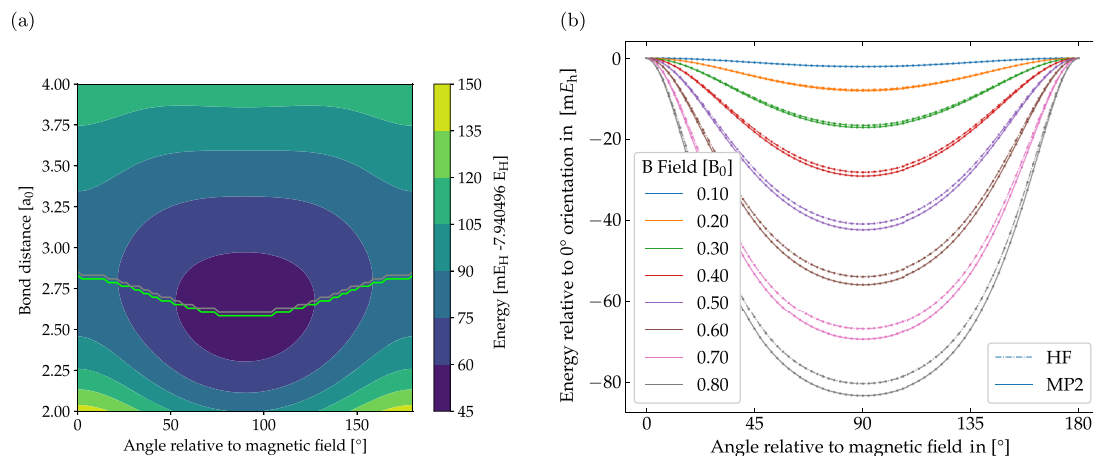


FIG. 8. (a) Potential energy surface of LiH for  $B = 0.2B_0$ . (b) Cosine-like potential for the equilibrium distance plotted against the angle.

for the Lorentz force, and as a consequence, any oscillation in a plane perpendicular to the field axis induces an intrinsic translation of the entire molecule in a direction perpendicular to both the bond axis and the field axis. It is important to note that the sign of this translational movement is not exclusively defined by the molecular properties as the initial velocities can also have a significant effect. Changing the sign of the initial velocities, for instance, will reverse the direction of this intrinsic translation.

The precession of  $H_2$  was a direct consequence of the fact that the nuclear charges are not entirely screened by the electrons of the

molecule. The same is true for LiH, and thus, a precession is obtained in a similar manner. However, this behavior is dependent on the nuclear kinetic energy of the system, and if it sinks below a certain limit, the precession is replaced by a more libration-like trajectory around the magnetic field axis. This is somewhat surprising since the molecule behaves as if it were interacting with an additional potential energy barrier for an orientation parallel to the direction of the intrinsic translation. The potential energy surface presented in Fig. 8, however, is invariant with respect to a rotation around the azimuthal angle. Even more surprisingly, once the barrier

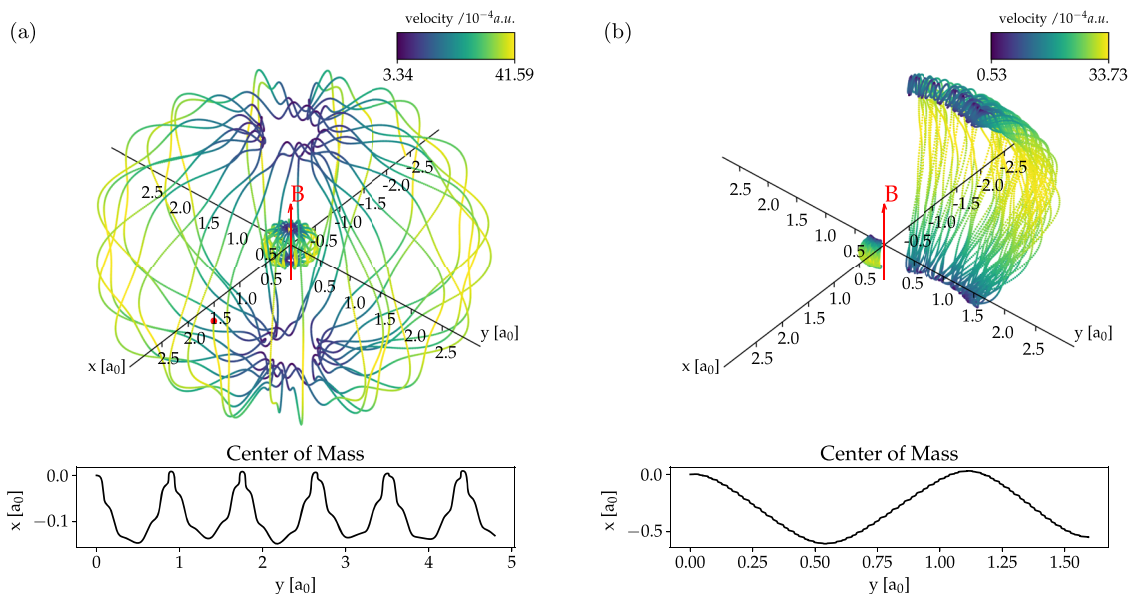


FIG. 9. More rotation-like trajectory (a) and more libration-like trajectory (b) at a magnetic field strength of  $0.2B_0$ . The center-of-mass motion has been purposefully eliminated here and is shown separately below the respective trajectories. Both simulations were initiated from the equilibrium geometry with the molecule oriented parallel to the  $x$  axis. Only the rotation around the  $y$  axis and the stretching vibration were given initial velocities.



is overcome, the molecule is free to rotate without any influence of this pseudopotential. A plausible explanation for this behavior is that the Lorentz force interacts with the pseudocharges of the permanent dipole moment while the aforementioned intrinsic translation is coupled to the center-of-mass movement of the molecule. The complex interaction between these two movements leads to the presence of a pseudopotential dependent on the initial conditions, and only one of these motions can relax at the same time. The consequence of this can be seen as a twitching in the intrinsic translation, which, thus, becomes more wave-like.

To summarize the differences between the nuclear dynamics of the hydrogen and lithium hydride molecules, the presence of a permanent dipole moment and a perpendicular equilibrium orientation leads to somewhat different trajectories for LiH. While for  $H_2$  a clear distinction between rotations and librations can be made, this is no longer possible for LiH. The precession around the field axis induced by Lorentz force and Berry curvature can be present for both molecules; however, for LiH, the nuclear kinetic energy needs to be above a certain threshold for this to occur. If the kinetic energy drops below this limit, LiH interacts with a velocity-dependent pseudopotential and rotation-like movements are replaced by more libration-like movements.

#### D. Rotational and vibrational spectrum of LiH

The LiH molecule possesses a permanent dipole moment. Therefore, we have not only computed power spectra from the nuclear velocities but also a spectrum from the time derivative of the dipole moment according to Eq. (10) of Ref. 60 (Fig. 10). For a spectrum corresponding to a more rotation-like movement, the rotational and vibrational spectra of LiH and  $H_2$  are very similar. Rotational overtones appear at every odd multiple of the fundamental frequency. In addition, couplings to the precession will split peaks corresponding to  $(x, y, z)$  components of the rotational movement into  $(x, y)$  multiplets and  $(z)$  singlets. Libration-like movements are, on the other hand, slightly different from  $H_2$ . Due to the in some way inverted potential barrier [see Figs. 2(b) and 8(b)],

the order of the peaks is also inverted. Therefore, peaks corresponding to the  $(z)$  component now occur at odd multiples of the fundamental frequency, and peaks corresponding to the  $(x, y)$  components can be found at even positions. This is summarized in the following patterns:

$$(x, y, z)^{\text{rot}} \rightarrow \underline{(x, y, z)}^{\pm}, \emptyset, (x, y, z)^{\pm}, \emptyset, \dots,$$

$$(x, y, z)^{\text{lib}} \rightarrow \underline{(z)}, (x, y)^{\pm}, \underline{(z)}, (x, y)^{\pm}, \dots$$

A similar coupling pattern is also found for the stretching vibration, where the additional Q-branch now corresponds to the  $(x, y)$  components,

$$(x, y, z)_{\text{sv}}^{\text{lib}} \rightarrow \dots, (x, y)^{\pm}, \underline{(z)}, \underline{(x, y)}^{\pm}, \underline{(z)}, (x, y)^{\pm}, \dots$$

Moving on, the effects of the precession and libration also differ from the  $H_2$  case, where it was responsible for a splitting of all frequencies active in the  $(x, y)^{\pm}$  component into doublets. For a more rotational-like movement, the fine structure of the peaks is analogous to the  $H_2$  molecule, and thus, all peaks corresponding to the  $(x, y)$  components of the movements are split into doublets. The precession itself is not visible in the power spectrum and only appears through its couplings.

For low nuclear kinetic energies, the precession is replaced by a libration-like movement. For an orientation parallel to the  $(x)$ -axis, the intrinsic translational movement points toward the  $(y)$  direction, and therefore, all peaks corresponding to the  $(y)$  component couple to an even multiple of the fundamental frequency of the precession. The peaks corresponding to the  $(x)$  component, however, couple to odd multiples of it. Thus, all peaks of the  $(x, y)$  components split into multiplets of alternating symmetry according to the following pattern:

$$(x, y)^{\pm} \rightarrow \dots, (x), (y), \underline{(x)}, (y), (x), \dots$$

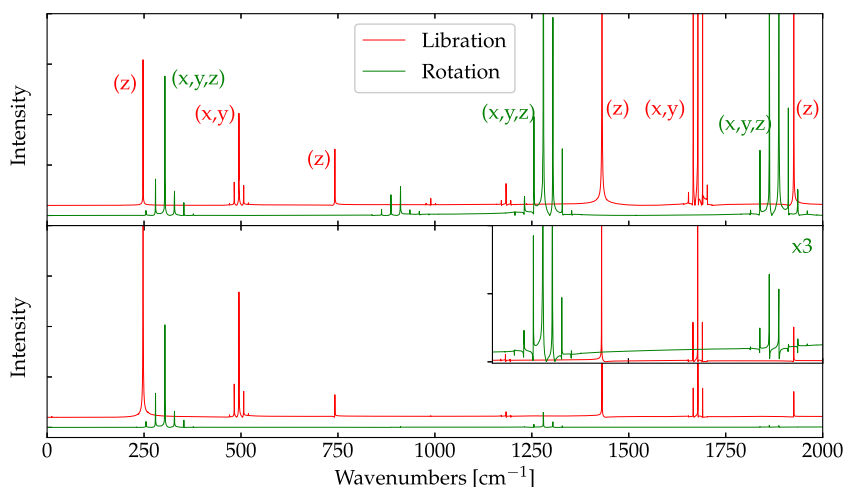


**FIG. 10.** Power spectrum obtained from nuclear velocities (top) and spectrum obtained from the time derivative of the dipole moment (bottom) for the LiH molecule in case of a rotation and a libration. The same initial conditions were used for the trajectories in Fig. 9, but the simulation time was set to 20 ps for a higher resolution of the Fourier transformation.

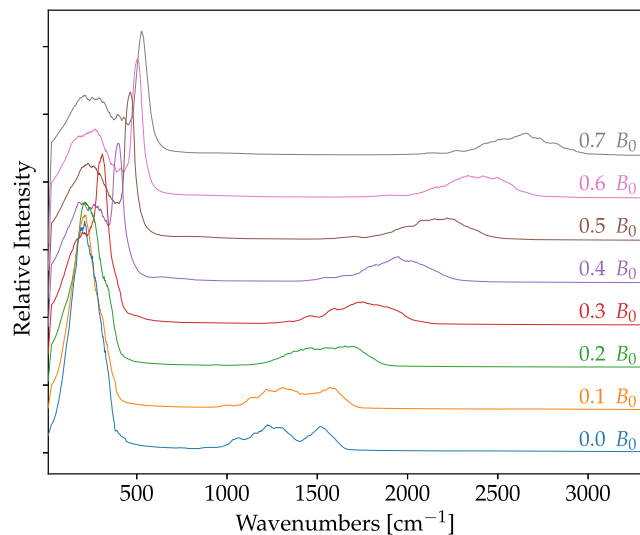


**FIG. 11.** Boltzmann averaged spectra (from nuclear velocities) from a set of 2000 LiH spectra in different field strengths. The initial velocities were chosen to yield a target temperature of 1500 K. The spectra were smoothed by averaging all frequencies within the interval  $\omega \pm 20 \text{ cm}^{-1}$ .

For an initial orientation of the molecule parallel to the ( $y$ ) axis, this pattern is simply inverted,

$$(x, y)^{\ddagger} \rightarrow \dots, (y), (x), (y), (x), (y), \dots$$

Here, the similarities to the stretching vibration become apparent as a peak of  $(x, y, z)_{sv}^{\text{lib}}$  character is coupling in a very similar manner.

### E. Canonical ensemble

In order to obtain a spectrum that is independent of the chosen set of initial conditions, a canonical ensemble from a set of 2000 spectra was calculated. For all simulations, the initial velocities were drawn from a Maxwell–Boltzmann distribution using a target temperature of 1500 K. In order to obtain a smoother spectrum, the wavenumber  $\omega$  was averaged over a constant interval ( $\omega \pm 20 \text{ cm}^{-1}$ ).

The field-free spectrum of LiH shows a strong rotational band and corresponding P- and R-branches for the stretching vibration (Fig. 11). As the magnetic field strength increases, the P- and R-branches broaden and an additional Q-branch appears, which cannot be resolved in detail. The stretching vibration itself (including P-, R-, and Q-branches) is blue-shifted for higher field strengths due to a sharper potential energy surface connected to the bond length. For field strengths greater than  $0.2B_0$ , libration-like movements begin to dominate the ensemble and their first overtones become clearly visible in form of a shoulder of the fundamental frequency.

### VI. CONCLUSION

In this work, we have presented a detailed analysis of *ab initio* molecular dynamics simulations for linear molecules in strong magnetic fields and investigated the rovibrational spectra of the  $\text{H}_2$

and LiH molecules. Nuclear trajectories were simulated using an adapted Tajima algorithm, which includes the screening of nuclear charges by the electrons through the inclusion of the Berry curvature tensor. Compared to the auxiliary coordinates and momenta (ACM) algorithm developed in previous work, the Tajima propagator is significantly more efficient without any loss of accuracy. In addition, no empirical coupling constant needs to be adjusted for the Tajima propagator, making it the algorithm of choice.

Rovibrational spectra of  $\text{H}_2$  and LiH in magnetic fields up to  $2B_0$  were simulated and carefully assessed. For molecular rotations, an energy barrier induced by the external field leads to hindered rotations (librations) at higher field strengths. The stretching vibration couples to rotations as well as to librations, but in a slightly different pattern since all nuclear motion has to be distinguished between different Cartesian components due to the broken isotropy of space. As a result, the coupling between stretching vibrations and rotational motion only results in P- and R-branches while an additional Q-branch becomes visible for coupling between vibrations and librations. The existence of a Q-branch may, therefore, be used as an indicator for librational motion at higher magnetic field strengths. Furthermore, rovibrational spectra exhibit signals belonging to precessions as previously observed for  $\text{H}_2$  as well as an intrinsic translation for molecules with permanent dipole moments such as LiH. All effects listed here as well as the increasing importance of rotational overtones in stronger fields are not only visible in individual spectra but also in canonical ensembles of spectra.

Having established the key components of calculating and interpreting rovibrational spectra in strong magnetic fields, the door is opened for further investigations on even larger systems. The effects of electron correlation beyond second-order perturbation theory on rovibrational spectra may also be of interest in future work. A fully quantum-mechanical treatment of rotational motion using, for instance, the rigid rotor approximation in a strong magnetic field could also provide more insight by including purely quantum effects such as nuclear tunneling.

### ACKNOWLEDGMENTS

A.P. acknowledges financial support by the Fonds der chemischen Industrie and Studienstiftung des deutschen Volkes. This work was supported by the Research Council of Norway through “Magnetic Chemistry” (Grant No. 287950) and the CoE Hylleraas Centre for Molecular Sciences (Grant No. 262695). L.M. thanks the Hylleraas Centre for hospitality and financial support during a 5-month visit there in 2020. In particular, the authors would like to thank Tanner Culpitt for fruitful discussion and helpful comments.

### AUTHOR DECLARATIONS

#### Conflict of Interest

The authors have no conflicts to disclose.

#### Author Contributions

**Laurenz Monzel:** Formal analysis (lead); Software (lead); Visualization (lead); Writing – original draft (lead). **Ansgar Pausch:**

Formal analysis (supporting); Software (equal); Writing – original draft (supporting). **Laurens D. M. Peters:** Formal analysis (equal); Methodology (equal); Software (equal); Writing – original draft (supporting). **Erik I. Tellgren:** Formal analysis (supporting); Methodology (supporting); Writing – review & editing (supporting). **Trygve Helgaker:** Conceptualization (lead); Funding acquisition (lead); Project administration (equal); Writing – original draft (supporting); Writing – review & editing (supporting). **Wim Klopper:** Conceptualization (supporting); Data curation (supporting); Formal analysis (supporting); Project administration (equal); Supervision (supporting); Writing – review & editing (supporting).

## DATA AVAILABILITY

The data that support the findings of this study are available from the corresponding author upon reasonable request.

## REFERENCES

- L. Ferrario, D. de Martino, and B. T. Gänsicke, *Space Sci. Rev.* **191**, 111 (2015).
- D. Lai, *Rev. Mod. Phys.* **73**, 629 (2001).
- F. Euchner, S. Jordan, K. Beuermann, K. Reinsch, and B. T. Gänsicke, *Astron. Astrophys.* **451**, 671 (2006).
- E. I. Tellgren, A. Soncini, and T. Helgaker, *J. Chem. Phys.* **129**, 154114 (2008).
- E. I. Tellgren, T. Helgaker, and A. Soncini, *Phys. Chem. Chem. Phys.* **11**, 5489 (2009).
- E. I. Tellgren, S. S. Reine, and T. Helgaker, *Phys. Chem. Chem. Phys.* **14**, 9492 (2012).
- G. David, T. J. P. Irons, A. E. A. Fouda, J. W. Furness, and A. M. Teale, *J. Chem. Theory Comput.* **17**, 5492 (2021).
- K. K. Lange, E. I. Tellgren, M. R. Hoffmann, and T. Helgaker, *Science* **337**, 327 (2012).
- J. Austad, A. Borgoo, E. I. Tellgren, and T. Helgaker, *Phys. Chem. Chem. Phys.* **22**, 23502 (2020).
- S. Stopkowicz, J. Gauss, K. K. Lange, E. I. Tellgren, and T. Helgaker, *J. Chem. Phys.* **143**, 074110 (2015).
- F. Hampe and S. Stopkowicz, *J. Chem. Phys.* **146**, 154105 (2017).
- F. Hampe and S. Stopkowicz, *J. Chem. Theory Comput.* **15**, 4036 (2019).
- F. Hampe, N. Gross, and S. Stopkowicz, *Phys. Chem. Chem. Phys.* **22**, 23522 (2020).
- E. I. Tellgren, A. M. Teale, J. W. Furness, K. K. Lange, U. Ekström, and T. Helgaker, *J. Chem. Phys.* **140**, 034101 (2014).
- J. W. Furness, J. Verbeke, E. I. Tellgren, S. Stopkowicz, U. Ekström, T. Helgaker, and A. M. Teale, *J. Chem. Theory Comput.* **11**, 4169 (2015).
- S. Reimann, A. Borgoo, E. I. Tellgren, A. M. Teale, and T. Helgaker, *J. Chem. Theory Comput.* **13**, 4089 (2017).
- T. J. P. Irons, L. Spence, G. David, B. T. Speake, T. Helgaker, and A. M. Teale, *J. Phys. Chem. A* **124**, 1321 (2020).
- T. J. P. Irons, G. David, and A. M. Teale, *J. Chem. Theory Comput.* **17**, 2166 (2021).
- C. Holzer, A. M. Teale, F. Hampe, S. Stopkowicz, T. Helgaker, and W. Klopper, *J. Chem. Phys.* **150**, 214112 (2019).
- C. Holzer, A. M. Teale, F. Hampe, S. Stopkowicz, T. Helgaker, and W. Klopper, *J. Chem. Phys.* **151**, 069902 (2019).
- C. Holzer, A. Pausch, and W. Klopper, *Front. Chem.* **9**, 746162 (2021).
- L. Adamowicz, E. I. Tellgren, and T. Helgaker, *Chem. Phys. Lett.* **639**, 295 (2015).
- L. Adamowicz, M. Stanke, E. Tellgren, and T. Helgaker, *Chem. Phys. Lett.* **682**, 87 (2017).
- L. Adamowicz, M. Stanke, E. Tellgren, and T. Helgaker, *J. Chem. Phys.* **149**, 244112 (2018).
- L. Adamowicz, M. Stanke, E. Tellgren, and T. Helgaker, *Chem. Phys. Lett.* **761**, 138041 (2020).
- M. J. Pemberton, T. J. P. Irons, T. Helgaker, and A. M. Teale, *J. Chem. Phys.* **156**, 204113 (2022).
- P. Schmelcher, L. S. Cederbaum, and H.-D. Meyer, *Phys. Rev. A* **38**, 6066 (1988).
- P. Schmelcher and L. S. Cederbaum, *Phys. Rev. A* **40**, 3515 (1989).
- P. Schmelcher and L. S. Cederbaum, *Int. J. Quantum Chem.* **64**, 501 (1997).
- Y. Li and C. A. Mead, *Theor. Chim. Acta* **82**, 397 (1992).
- C. A. Mead, *Rev. Mod. Phys.* **64**, 51 (1992).
- L. Yin and C. A. Mead, *J. Chem. Phys.* **100**, 8125 (1994).
- D. Ceresoli, R. Marchetti, and E. Tosatti, *Phys. Rev. B* **75**, 161101 (2007).
- T. Culpitt, L. D. M. Peters, E. I. Tellgren, and T. Helgaker, *J. Chem. Phys.* **155**, 024104 (2021).
- L. D. M. Peters, T. Culpitt, L. Monzel, E. I. Tellgren, and T. Helgaker, *J. Chem. Phys.* **155**, 024105 (2021).
- T. Culpitt, L. D. M. Peters, E. I. Tellgren, and T. Helgaker, *J. Chem. Phys.* **156**, 044121 (2022).
- F. London, *J. Phys. Radium* **8**, 397 (1937).
- R. Ditchfield, *Mol. Phys.* **27**, 789 (1974).
- T. J. P. Irons, J. Zemen, and A. M. Teale, *J. Chem. Theory Comput.* **13**, 3636 (2017).
- J. I. Rawlinson and C. Tronci, *Phys. Rev. A* **102**, 032811 (2020).
- L. Verlet, *Phys. Rev.* **159**, 98 (1967).
- S. Blanes and P. C. Moan, *J. Comput. Appl. Math.* **142**, 313 (2002).
- E. Forest and R. D. Ruth, *Physica D* **43**, 105 (1990).
- M. Tao, *J. Comput. Phys.* **327**, 245–251 (2016).
- M. Tao, *Phys. Rev. E* **94**, 043303 (2016).
- T. Tajima, *Computational Plasma Physics: With Applications to Fusion and Astrophysics* (CRC Press, 2018).
- R. Ahlrichs, M. Bär, M. Häser, H. Horn, and C. Kölmel, *Chem. Phys. Lett.* **162**, 165 (1989).
- F. Furche, R. Ahlrichs, C. Hättig, W. Klopper, M. Sierka, and F. Weigend, *Wiley Interdiscip. Rev.: Comput. Mol. Sci.* **4**, 91 (2014).
- TURBOMOLE V7.5 2020, a development of University of Karlsruhe and Forschungszentrum Karlsruhe GmbH, 1989–2007, TURBOMOLE GmbH, since 2007; available from <http://www.turbomole.com>.
- A. Pausch and W. Klopper, *Mol. Phys.* **118**, e1736675 (2020).
- S. Sun, D. B. Williams-Young, T. F. Stetina, and X. Li, *J. Chem. Theory Comput.* **15**, 348 (2018).
- M.-P. Kitsaras and S. Stopkowicz, *J. Chem. Phys.* **154**, 131101 (2021).
- C. Hättig and F. Weigend, *J. Chem. Phys.* **113**, 5154 (2000).
- K. Krause and W. Klopper, *J. Chem. Phys.* **142**, 104109 (2015).
- F. Weigend and R. Ahlrichs, *Phys. Chem. Chem. Phys.* **7**, 3297 (2005).
- F. Weigend, *Phys. Chem. Chem. Phys.* **8**, 1057 (2006).
- F. Weigend, M. Häser, H. Patzelt, and R. Ahlrichs, *Chem. Phys. Lett.* **294**, 143 (1998).
- E. Kestemont and J. Van Craen, *J. Comput. Phys.* **22**, 451 (1976).
- M.-P. Gageot, M. Martinez, and R. Vuilleumier, *Mol. Phys.* **105**, 2857 (2007).
- M. Thomas, M. Brehm, R. Fligg, P. Vöhringer, and B. Kirchner, *Phys. Chem. Chem. Phys.* **15**, 6608 (2013).
- P. H. Berens and K. R. Wilson, *J. Chem. Phys.* **74**, 4872 (1981).
- P. Schmelcher and L. S. Cederbaum, *Phys. Rev. A* **41**, 4936 (1990).
- A. Pausch, M. Gebele, and W. Klopper, *J. Chem. Phys.* **155**, 201101 (2021).